Structure Function Ratios
Recent Results from NMC

Margriet van der Heijden
NIKHEF-K
Amsterdam

Christoph Scholz
Max-Planck-Institut für Kernphysik
Heidelberg

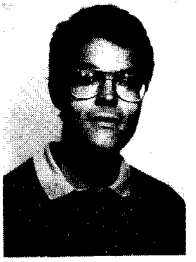

Abstract

Ratios of structure functions are determined in measurements of deep inelastic muon scattering. The ratio $F_2^n/F_2^p(x)$ has been measured using hydrogen and deuterium targets and incoming muons with energies of 274 GeV and 89 GeV. The ratios F_2^{He}/F_2^D, F_2^C/F_2^D and F_2^{Ca}/F_2^D have been measured at 197 GeV. The measurements cover a wide range in x and Q^2. Due to a complementary target system systematic errors are small.

The ratio $F_2^n/F_2^p(x)$, together with a deuteron structure function obtained from a fit to the world data, is also used to calculate the Gottfried sum rule.

With the heavy target data the variation of the EMC effect with A and the momentum conservation sum rule are studied.

1 Introduction

In the quark parton model (QPM) the structure function F_2 can be interpreted in terms of quark distributions. Within this model the ratio F_2^n/F_2^p depends in the large-x region on the ratio of valence quark distributions. In the low-x region, where sea quarks dominate, the ratio is affected by the residual valence quark distributions and by a possible flavour symmetry breaking in the sea. The ratio F_2^n/F_2^p thus puts constraints on the quark distributions. One of the aims of the NMC experiment is to measure the ratio F_2^n/F_2^p in a wide range of x and Q^2 with high statistical and systematic accuracy. The present data extend to lower x values than data from previous experiments.

Furthermore we measured the structure function[1] ratio F_2^A/F_2^D, where A is a heavy nucleus, in order to investigate the EMC effect. It is now well established that the nuclear environment influences the structure functions of nucleons. However, the experimental information, especially at low x, is not sufficiently precise to distinguish between the various theoretical models. Helium, carbon and calcium are isoscalar nuclei with the maximum possible variation in mass number. The binding energies per nucleon and the nucleon densities in the three nuclei are similar. If the EMC effect predominantly depends on binding, it should be similar for these three nuclei, as it appears at large x. Dependence on the volume, however, would imply considerable differences.

2 The detector

The experiment was performed at the M2 muon beam line of the CERN SPS. The measurements on hydrogen and deuterium were done using incoming muons with an energy of 274 GeV and 89 GeV. In the case of He, C, Ca the energy was 197 GeV. The rms energy spread was 4 % of the incident energy.

The detector used in these measurement was the upgraded version [1,2] of the EMC apparatus [3]. A small angle trigger was used parallel to the standard physics trigger. The acceptance thus extends down to a scattering angle of 5 $mrad$.

An important reduction of the systematic errors due to acceptance and normalisation uncertainties is obtained by the use of a complementary target system. Two different target materials (A, B), positioned one behind the other, are simultaneously exposed to the beam. Since the beam flux is the same for both targets, the flux normalisation cancels. The acceptance of the spectrometer depends strongly on the vertex position and is thus different for the two targets. The target pair is therefore exchanged with a second pair in which the sequence of target materials is inverted. In order to reduce effects that might arise from variations of the acceptance with time, the target pairs were interchanged frequently, typically twice per hour.

[1]Throughout this paper F_2^D, F_2^A etc. denotes the structure function normalised to the number of nucleons

The experimental cross section ratio therefore only depends on the number of events N and the number of nucleons per area T in the upstream and downstream targets:

$$\frac{\sigma^A_{exp}}{\sigma^B_{exp}} = \sqrt{\frac{N^A_u \cdot N^A_d}{N^B_u \cdot N^B_d} \Big/ \frac{T^A_u \cdot T^A_d}{T^B_u \cdot T^B_d}} \tag{1}$$

In the H–D and the He–D measurement $3\,m$ long liquid targets were used. In the case of C–D and Ca–D the liquid D_2 targets were $1.1\,m$ long. The thicknesses of the C and Ca targets were similar to the thickness of the D_2 targets. They consisted of several equally spaced slices, which were regularly distributed over a region of $1.1\,m$, in order to obtain approximately the same spatial mass distributions.

3 Data Selection and Processing

The data were reconstructed using the upgraded EMC analysis chain [1,3,4]. To limit the size of the radiative corrections and to remove contamination from hadronic decays, kinematic cuts were applied to the data. Cuts to remove events from regions with rapidly changing acceptances and lower spectrometer resolution are loosened considerably with respect to previous measurements. This is because acceptances cancel in the ratios of the cross sections due to the target system.

To extract the ratios of one-photon cross sections from the ratios of the measured cross sections radiative correction factors $\eta = \sigma_{1\gamma}/\sigma_{exp}$ were applied to each event. These correction factors were calculated according to the formalism of Mo and Tsai [5]. The absolute structure functions F_2^p, F_2^D and F_2^A ($A = He,\ C,\ Ca$) play an essential rôle in the calculation. F_2^D is determined from a fit to all available muon and electron scattering data down to the inelastic threshold [6]. To obtain F_2^A the F_2^D fit was multiplied with the ratio F_2^A/F_2^D taken from the present data for lower x and from SLAC data [7] for $x > 0.4$. The measured ratio F_2^p/F_2^D was used together with the F_2^D fit to obtain F_2^p in the kinematic region that is covered by our data. An iterative procedure is thus required, which converges after about four steps. The advantage of this method is that the uncertainties due to normalisation of the absolute structure functions are common for F_2^p, F_2^A and F_2^D. Therefore the radiative corrections for all nuclei are affected in a similar way, and the errors due to this normalisation cancel in part in the ratio.

The one-photon cross section for the deep inelastic charged lepton scattering process depends not only on F_2 but also on R. Here R is the ratio of the absorption cross sections of longitudinally and transversely polarised virtual photons. Assuming that R is the same for the different target nuclei, which is consistent with data from SLAC [8,9], the structure function ratios are equal to the cross section ratios.

4 Systematic Uncertainties

Systematic uncertainties arise from: i) radiative corrections, ii) momentum determination, iii) vertex smearing and density of the targets, iv) limited spectrometer resolution (smearing).

i) The uncertainty in the radiative corrections affects the data at low x. It is mainly due to the normalisation uncertainty of F_2 and to the incomplete knowledge of R and the suppression factors. For 89 GeV muons, the uncertainty in the radiative corrections is dominated by the lack of knowledge of R at low Q^2. For 274 GeV muons the uncertainty of the suppression factors is the most important.

ii) The uncertainty in the determination of the momenta of incoming and scattered muons is a consequence of the error of the calibration of the magnets. It affects the data at high x.

iii) Fiducial cuts are applied to the vertex distributions to minimise the number of events that are lost or wrongly assigned to a target. The error on the calculation of the tails of the vertex distributions produces a systematic uncertainty in the data, which is largest at small x. Small uncertainties come from the uncertainty in the target densities and the HD admixture in the D_2 target.

iv) The effects of the limited detector resolution on the ratio were studied with the Monte Carlo simulation of the experiment and turned out to be small. The effects on the ratio of background in the apparatus and multiple Coulomb scattering in the targets are negligible.

The individual contributions were added in quadrature to obtain the total systematic error.

5 Results from Hydrogen and Deuterium

Neglecting effects from nuclear binding, the cross section for scattering on deuterons is equal to the sum of the cross sections for scattering on free protons and neutrons. Consequently, the ratio F_2^n/F_2^p is defined as:

$$\frac{F_2^n}{F_2^p} = \frac{2F_2^D}{F_2^p} - 1 \quad . \tag{2}$$

No corrections for the Fermi motion of the proton and the neutron in the deuteron are made. These corrections are negligible at $x < 0.6$.

The result from 274 GeV muons is obtained with roughly half of the available data. It covers the kinematic range $x = 0.004 - 0.8$ with $1 < Q^2 < 5 GeV^2$ for the lowest and $10 < Q^2 < 190 GeV^2$ for the highest x bin. The result from 89 GeV muons covers the range $x = 0.004 - 0.7$ with $0.5 < Q^2 < 1.1 GeV^2$ for the lowest and $7 < Q^2 < 26 GeV^2$ for the highest x bin.

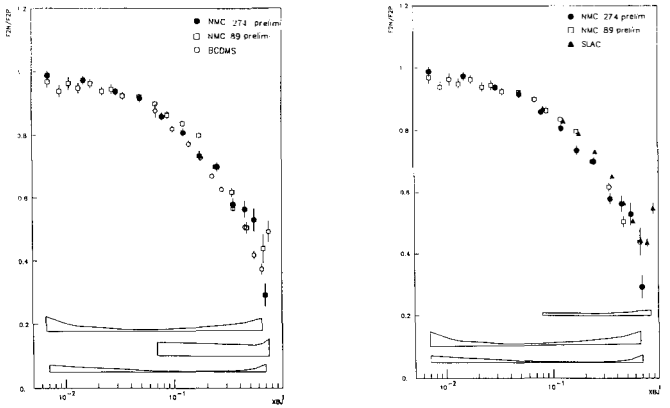

Figure 1: (a) F_2^n/F_2^p from NMC and BCDMS [11]; (b) F_2^n/F_2^p from NMC and SLAC [9] .

Ratios

The results from the measurements with 274 GeV and 89 GeV muons are shown in figure 1a,b. The measurement with 89 GeV muons covers a region of smaller Q^2. Previously, the ratio has been measured with high energy muon beams at CERN by EMC and BCDMS [10,11]. Using electron scattering it has also been measured at SLAC [12]. In figure 1a the results are shown together with the BCDMS data. Similar Q^2 ranges are covered by the BCDMS experiment and by the present measurement with 274 GeV muons. The results are in good agreement in the region of overlap. Our data extend to smaller x and have smaller systematic errors. The BCDMS result is more precise in the region $x > 0.3$. The two results together cover a large x range with high precision.

The present result from 89 GeV muons covers approximately the same Q^2 region as the SLAC data (0.6-30 GeV^2). The SLAC result and the present one at 89 GeV are different from the high energy results, indicating a Q^2-dependence of F_2^n/F_2^p (figure 1b).

The results extend below $x = 0.03$ covering the region where the sea partons dominate. The data points at low x are consistent with the QPM prediction $F_2^n/F_2^p = 1$ at $x = 0$.

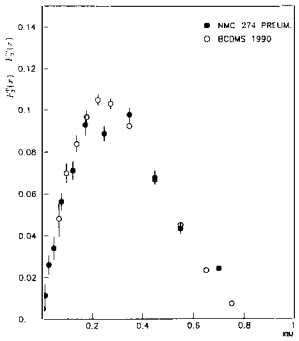

Figure 2: $F_2^p - F_2^n$ obtained from F_2^n/F_2^p at 279 GeV and F_2^D fit.

Gottfried sum rule

The ratio, together with F_2^D obtained from a fit to all available electron and muon data [6], was also used to calculate the difference of the structure functions $F_2^p - F_2^n$ from

$$F_2^p - F_2^n = 2F_2^D \cdot \frac{1 - F_2^n/F_2^p}{1 + F_2^n/F_2^p} \tag{3}$$

The quantity $F_2^p - F_2^n$ is used in the Gottfried sum rule [13]. Two assumptions are made. Firstly, the proton and neutron form an isospin doublet. Secondly, the sea in proton and neutron is flavour symmetric. Under these assumptions and in the framework of the QPM, the sum rule predicts [14]:

$$\int_0^1 \frac{F_2^p - F_2^n}{x} dx = \frac{1}{3} \ . \tag{4}$$

Perturbative QCD corrections to the sum rule are negligible [15]. The $1/x$ term in the integral leads to a large contribution from the small-x region, which is not covered by previous experiments. However, using the present result on F_2^n/F_2^p together with the F_2^D fit allows one to integrate down to $x = 0.004$. The resulting value of the integral is:

$$\int_{0.004}^{0.8} \frac{F_2^p - F_2^n}{x} dx = 0.219 \pm 0.008\,(\text{stat}) \pm 0.021\,(\text{syst}) \tag{5}$$

at $Q^2 = 15\ GeV^2$. Any possible Q^2 dependence in the ratio is neglected.

The systematic error on the integral arises from: i) the systematic uncertainties on the ratio, ii) the systematic uncertainty on the F_2^D fit.

i) The sources of uncertainties on the ratios and their effect on the integral are listed in table 1. The total error is taken to be the quadratic sum.

ii) The error on the F_2^D fit is estimated to be 5% in the region $x = 0.1 - 0.8$ where it is mainly due to the uncertainty in the normalisation. It is increasing at lower x values; at $x = 0.004$ it is 11 %. The error on the F_2^D fit gives rise to an uncertainty on the integral of 6 %.

Both uncertainties are added in quadrature.

To estimate the contributions from the low x and high x regions, $F_2^p - F_2^n$ is extrapolated to $x = 0$ and $x = 1$. The contribution from the high x region is negligible. In the small x region $F_2^p - F_2^n$ is assumed to have Regge behaviour and is taken to be proportional to x^α with $\alpha = 0.5$. This leads to a contribution to the integral of 0.010. Choosing $\alpha = 0.3$, and 0.7 [11] the contributions are 0.020 and 0.004, respectively. Another estimate of the contributions from the low-x and high-x regions is obtained by extrapolating the measured ratio to $x = 0$ and $x = 1$ and calculating $F_2^p - F_2^n$ according to eq. 3. The fit to the ratio is made with the constraint that $F_2^n/F_2^p = 1$ at $x = 0$. The contribution from the high-x region is negligible. The contribution from the small-x region varies between 0.003 and 0.004. This variation is mainly due to the uncertainty on the F_2^D fit in the small-x region.

A Q^2-dependence of the ratio would affect the result obtained with this method. The effect is estimated to be small and it slightly decreases the value of the integral quoted in eq. 5.

The calculated structure function difference $F_2^p - F_2^n$ is shown in figure 2. The cumulative plot of figure 3 gives an insight into the contributions of the different x bins to the integral.

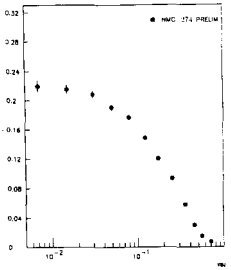

Figure 3: Cumulative integral $\int_x^{0.8}(F_2^p - F_2^n)/x'\,dx'$ as a function of x.

Source of error on F_2^n/F_2^p	Error on integral
Radiative corrections:	
— Normalisation of F_2^D	0.007
— Suppression of electric form factor	0.009
— Suppression of magnetic form factor	0.009
— Uncertainty in R	0.001
Density of targets	0.002
HD admixture in D_2 target	0.003
Smearing of vertex variables	0.006
Smearing of kinematic variables	0.000
Momentum determination	0.002
Quadratic sum	0.016

Table 1: Contributions to the systematic error on the integral.

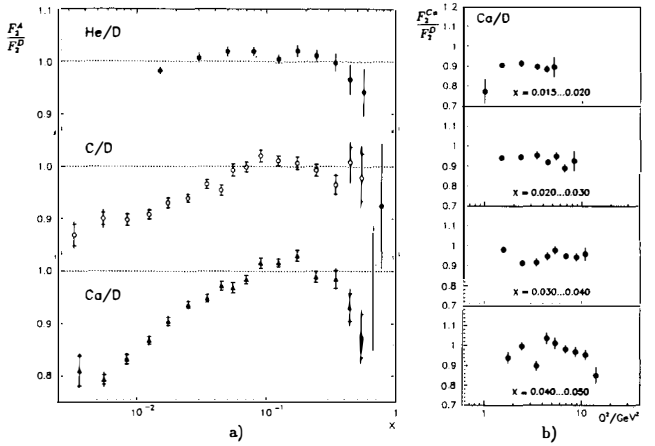

Figure 4: (a)Structure function ratios F_2^A/F_2^D as function of x averaged over Q^2. The inner error bars are statistical only, the outer error bars include the systematic errors added in quadrature. (b) Q^2 dependence of the structure function ratio F_2^{Ca}/F_2^D for four different x bins. The error bars denote the statistical errors only.

6 Results for the heavy targets

The results of F_2^A/F_2^D are presented in figure 4a as a function of x, averaged over Q^2. The results cover the kinematical range $x = 0.0035 - 0.7$ and $Q^2 = 0.7 - 90\ GeV^2$. The inner error bars in the figure are the statistical errors only, the outer error bars include the systematic error added in quadrature. For F_2^{He}/F_2^D statistical errors are shown only.

The three structure function ratios show a characteristic x dependence. There is a depletion below unity at low x, which increases with decreasing x. This depletion is more pronounced at larger A and reaches a value of 4 %, 10 %, 20 % below unity for He, C and Ca. The depletion is followed by an enhancement at intermediate x. Its onset is shifted towards higher x as the mass number increases ($x \approx 0.025, 0.063, 0.076$). The enhancement reaches a maximum value of $\approx 2\,\%$ above unity for the three ratios. In the large x region ($x \gtrsim 0.3$) the present data are consistent with the well established depletion of the EMC effect [7].

Throughout the accessible Q^2 range there is no indication for any Q^2 dependence of the EMC effect. As an example figure 4b shows F_2^{Ca}/F_2^D as a function of Q^2 for several x bins.

From the structure function ratios and the knowledge of the absolute structure function F_2^D the structure function difference can be evaluated as

$$F_2^A - F_2^D = \left(\frac{F_2^A}{F_2^D} - 1\right) \cdot F_2^D(x) \quad . \tag{6}$$

Taking the present data for $x < 0.4$ and the SLAC data [7] for higher x, the integral can be evaluated through the accessible x-range (0.005 – 0.78). The extrapolation to the entire x region gives a correction which is small. The absolute structure function F_2^D is taken at Q^2=4 GeV^2, which is a typical value for both data sets.

After a correction for the mass defect of bound nucleons the results normalised to $N = \int_0^1 F_2^D(x)dx$ are:

$$\begin{aligned}
\frac{1}{N}\int_0^1 F_2^{He} - F_2^D(x)\,dx &= -0.3 \pm 0.3\ (\text{stat}) \pm (?)\,\%\ (\text{syst}) \\
\frac{1}{N}\int_0^1 F_2^{C} - F_2^D(x)\,dx &= -1.7 \pm 0.4\ (\text{stat}) \pm 0.8\,\%\ (\text{syst}) \\
\frac{1}{N}\int_0^1 F_2^{Ca} - F_2^D(x)\,dx &= -2.3 \pm 0.4\ (\text{stat}) \pm 0.7\,\%\ (\text{syst})
\end{aligned}$$

In the framework of the parton model this can be interpreted as a reduction of the longitudinal momentum fraction in the heavier nuclei carried by charged partons.

7 Summary

The ratio of structure functions $F_2^n/F_2^p(x)$ has been determined down to $x = 0.007$ at incoming muon energies of 89 GeV and 274 GeV. The statistical and systematic accuracy is high. At smallest x the ratio is close to unity. The comparison of the results at 89 GeV and 274 GeV indicates a non-zero Q^2 dependence of the ratio. The ratio is used, together with the deuteron structure function obtained from a fit to the world data, to calculate the Gottfried sum rule. The result obtained in this way (eq. 5) is not in agreement with the predictions from the QPM and perturbative QCD.

In the heavy target experiments we have measured the x, A and Q^2 dependence of the EMC effect at small x. The depletion at low x turned out to be strongly A dependent, in contrast to the enhancement at higher x. The onset of the enhancement is shifted towards higher values of x with increasing mass number A. For all three structure function ratios no Q^2 dependence is observed. There are indications that the integrals of $F_2^A - F_2^D$ slightly decreases with increasing mass number A.

References

[1] C. Broggini, Ph.D. thesis, University of Neuchâtel (1989)
D. Nowotny, Ph.D. thesis, University of Heidelberg (1989)
A. Simon, Ph.D. thesis, University of Heidelberg (1988)
C. Scholz, Ph.D. thesis, University of Heidelberg (1989)

[2] D. Allasia *et al.* (EMC), CERN-SPS 85–18 (1985)

[3] O. C. Allkofer *et al.* (EMC), Nucl. Instr. & Meth. **179** (1981) 445

[4] J. P. Albanese *et al.* (EMC), Nucl. Instr. & Meth. **212** (1983) 111

[5] L. W. Mo and Y. S. Tsai, Rev. Mod. Phys. **41** (1969) 205
Y. S. Tsai, SLAC-PUB-848 (1971)

[6] Y. Mizuno, to be published

[7] R.G.Arnold *et al.* (SLAC E139), Phys. Rev. Lett. **52** (1984) 727

[8] J. Dasu *et al.* (SLAC E140), Phys. Rev. Lett. **60** (1988) 2593

[9] L. W. Whitlow, Ph.D. Thesis, Stanford University (1990), SLAC-Report 357 (1990)

[10] J. J. Aubert *et al.* (EMC), Nucl. Phys. **B293** (1987) 740

[11] A. C. Benvenuti *et al.* (BCDMS) , Phys. Lett. **B237** (1990) 599

[12] A. Bodek *et al.*, Phys. Rev. **D20** (1979) 1471

[13] K. Gottfried, Phys. Rev. Lett. **18** (1967) 1174

[14] D.Allasia *et al.*, Phys. Lett. **135B** (1984) 231

[15] C. Lopez and F. J. Yndurain, Nucl. Phys. **B183** (1981) 157
D. A. Ross and C. T. Sachrajda, Nucl. Phys. **B149** (1979) 497